Desalination and Water Treatment
www.deswater.com

doi: 10.5004/dwt.2023.29296

285 (2023) 36–46
February

Residence time distribution in reverse osmosis/nanofiltration spiral-wound modules in a laboratory scale desalination unit

S. Chamam, A. Hannachi*

Research Laboratory of Process Engineering and Industrial Systems, National Engineering School of Gabes, University of Gabes, Omar Ibn El Khattab Street, 6029 Zrig, Gabes, Tunisia, emails: ahmed.hannachi@enig.rnu.tn (A. Hannachi), sabrine.chamam@univgb.tn (S. Chamam)

Received 30 September 2022; Accepted 27 December 2022

ABSTRACT

Membrane processes are dominating desalination techniques. Reverse osmosis (RO) is currently the most used technique for seawater and brackish water desalination. Nanofiltration (NF) could be an interesting alternative option for brackish water desalination. As global warming unleashes its disastrous impact on freshwater availability, desalination techniques are helping ensuring water supplies cover the increasing demand for drinking and all economic sectors. The overall performances of such membrane processes depend on many factors. Flow hydrodynamics within membrane modules is particularly critical for ensuring better salt retention, higher recovery rate, and longer module life span by helping preventing scaling and fouling. In this work, we attempted to determine the residence time distribution as a flow hydrodynamics characterization method in spiral-wound membrane modules. The experimental work was performed on RO and NF modules of a laboratory scale unit. It proved that RO modules have better mixing quality compared to the case of NF which have a shorter mean residence time. It also confirmed that increasing the applied pressure, within the considered experimental domain, leads to better flow patterns approaching plug flow configuration.

Keywords: Desalination; Spiral-wound modules; Reverse osmosis; Nanofiltration; Flow Hydrodynamics; Residence time distribution

1. Introduction

Only 2.5% of the global water can be qualified as freshwater, whereas the rest is saline. Adding to that, the decline of resources in some places of the globe and the significant rise in human population intensified the water demand and reduced its accessibility. Moreover, several natural water bodies have been contaminated with elements that may induce serious health problems, such as organic matter, arsenic, and fluoride. According to the United Nations, over two billion people live in countries undergoing water stress [1]. Desalination offers a solution to the rising water scarcity, helping achieving water sustainability and addressing future water availability challenges. It provides additional water resources for human use in water-stressed areas and alleviates the burden on freshwater resources in regions with water pollution or groundwater over-exploitation problems [2,3]. Water desalination processes require significant quantities of energy to achieve salt separation from the recovered fresh water. The amount and type of energy differ according to the employed technique. Currently, membrane-based desalination processes have overtaken thermal processes due to their lower operating and investment costs [4].

Reverse osmosis (RO) and the newly emerged nanofiltration (NF), two pressure-driven processes, are commonly adopted to produce fresh water from brackish or seawater. Reverse osmosis processes use semi-permeable membranes with the smallest pore sizes and the highest applied pressure compared to other membrane technologies. Today,

* Corresponding author.

about 80% of the world's installed desalination plants use RO processes [5]. Nanofiltration offers membrane properties between ultrafiltration (UF) and reverse osmosis (RO). As a singular process, it proved to be ineffective to reach the drinking water standards when treating seawater, but it was successful in the case of mildly brackish feed water [6–8]. Key distinguishing characteristics of NF membranes are the low rejection of monovalent ions, high rejection of divalent ions and higher permeate flux, and also the lower operating pressures compared to RO membranes [3].

Despite the significant development in NF and RO, there are still some drawbacks, mainly due to membrane fouling, which drastically affects operation performance and maintenance costs [9–11]. The main critical fouling in membrane-based desalination processes is inorganic, referred to as scaling. As a result of membrane selectivity, there is a build-up of ionic species on the membrane surface of the retentate side, known as concentration polarization. This accretion may allow reaching supersaturations with respect to some sparingly soluble salts such as $CaCO_3$ and $CaSO_4$. These salts may crystallize within membrane modules inducing a decline in performances and perhaps a drastic drop of modules' life span. Several techniques are used to control the scale formation, such as altering the feed characteristics (pH, antiscalant injection dosing), and optimizing the process design and operating parameters. However, inorganic fouling is yet present in membrane-based desalination processes [12,13]. Flow hydrodynamics within membrane modules have a significant influence on desalination performances. They affect all species transport phenomena parallel and cross the membrane active layer influencing fouling occurrences. Controlling fouling requires pursuing a favorable flow pattern along membrane modules and pressure vessels in desalination units. Determination of the residence time distribution (RTD) is a means to examine flow behavior inside membrane modules [14,15]. Roth et al. [16] suggested this method for screening membrane fouling using the following steps. A tracer is injected at the module entrance in a pulse or a step-wise form. The tracer material can be a dye or a conductive solution. Then the time response at the module exit is monitored. The response signal is then analyzed to determine the mean residence time, the presence of dead volumes, and the intensity of mixing [15,17–21]. Many studies adopted this approach to monitor process performances and annotate the experimental data until tracer flushing [16–21]. Recently, RTD was calculated using computational fluid dynamics to determine the effect of RO flushing [22]. Several RTD studies in membrane desalination processes are reported in Table 1.

The RTD helps understanding desalination systems' performances and facilitates the detection of any membrane module abnormalities. Several theoretical models were used to describe the resident time and define its parameters in order to determine its distribution and its fitting by well-known behaviors, such as the tank-in-series model, the axial dispersion model, and the exponentially modified Gaussian model [22–25]. This allows as well modeling the module through a series of communicating continuous stirred tank reactor CSTR, with or without dead volumes. This approach also helps determining the prevailing dispersion models in membrane modules.

As tap water quality does not often meet WHO requirements, the use of membrane desalination units has extended to domestic sizes for everyday household use. However, the flow hydrodynamics and the fouling effects on the membrane performances of these small units remain unclear. This study intends to unfold the RTD at several applied pressure as a flow hydrodynamics characterization method in spiral-wound membrane modules. The experimental work was conducted on RO and NF modules of a small-size laboratory-scale unit. Moreover, the tracer used is a macromolecule that is totally rejected by membranes giving much better insights on RTD than previous investigations based on the use of soluble salts partially retained by desalination membranes.

2. Materials and methods

2.1. Experimental setup

A laboratory-scale pilot, shown in Fig. 1, was used to conduct various tests. Two main sets of experiments were carried out to determine the RTD. The first set was for a commercial spiral Aquapro RO membrane. The second set concerned a commercial NF membrane provided by Membranuim® [26,27]. These tests were realized at several trans-membrane pressures using pure water as the feed solution. The used tracer is an industrial fluorescent solution provided by Nalco and is well-known as a scale chemical for RO and boilers.

The unit performances were supervised using conductivity meters, flow meters (FI), and manometers (PI). The recovery rate R is calculated as:

Table 1
RTD studies in the field of membrane desalination reported in the literature

Membrane type	Tracer	Injection type	References
RO	NaCl	Pulse	[16]
NF/RO	NaCl, $CaCl_2$, and $Cu(NO_3)_2$	Pulse	[17]
RO	NaCl	Pulse	[18]
RO	NaCl	Pulse	[19]
UF	Fluorescent $C_{20}H_{12}O_5$	Pulse	[20]
RO	Virtual (simulation CFD)	Pulse	[22]
RO/NF	PermaTreat® PC-191T	Pulse	Present work

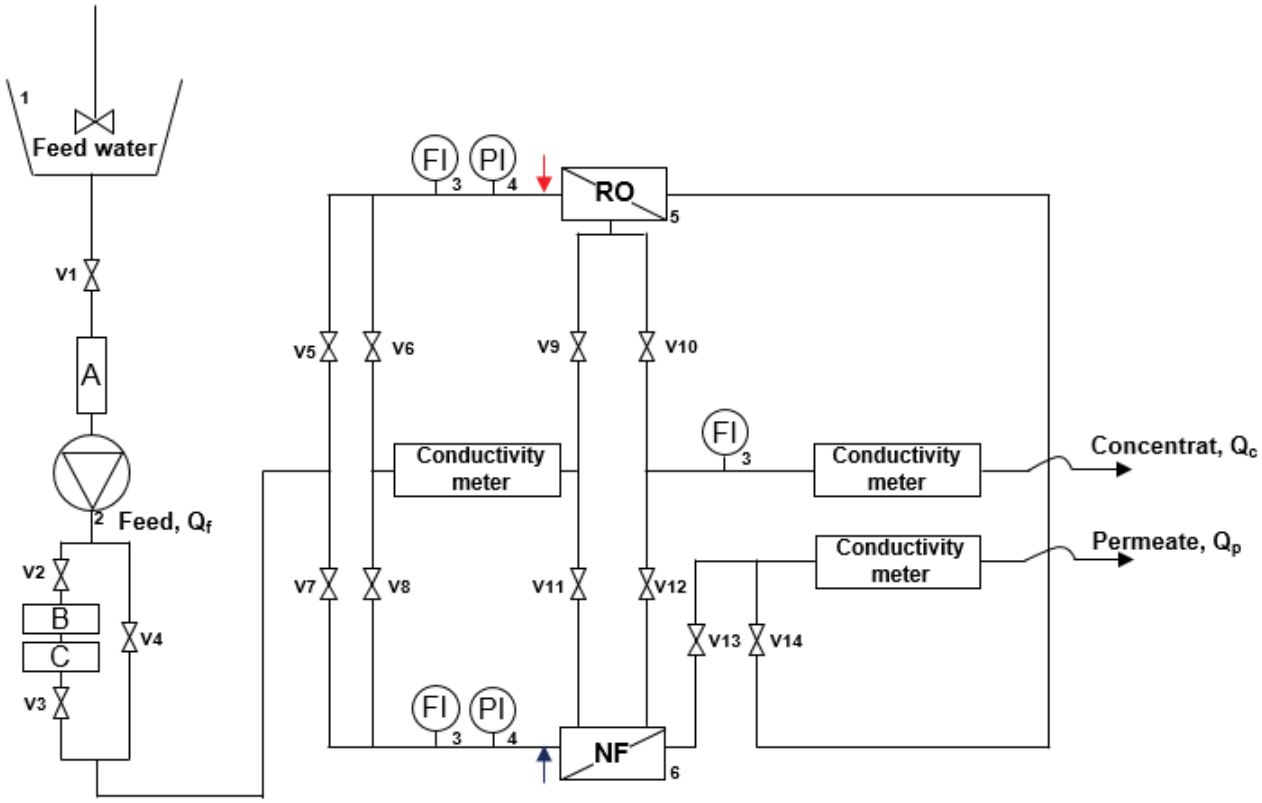

Fig. 1. Schematic representation of the laboratory scale pilot.

$$R = \frac{Q_p}{Q_f} \tag{1}$$

where Q_f and Q_p are the feed and the permeate flow rates, respectively. With

$$Q_f = Q_p + Q_e \tag{2}$$

where Q_c is the concentrate flow rate.

2.2. Product and analytical tools

Distilled water filtrated through membrane modules is used as a feed solution. Its conductivity is below 10 μS/cm. The employed tracer is a commercial scale inhibitor, PermaTreat® PC-191T, developed by Nalco water for reverse osmosis (RO) systems. It is a non-invasive tracer that cannot permeate through the membrane. The tracer content at the concentrate side was observed using a TRASAR® Pen Fluorometer provided by Nalco water. Fig. 2 represents the calibration curve of the tracer solution at different concentrations (C_t) and the measured concentrations ($\hat{C}_t$) by the pen fluorometer.

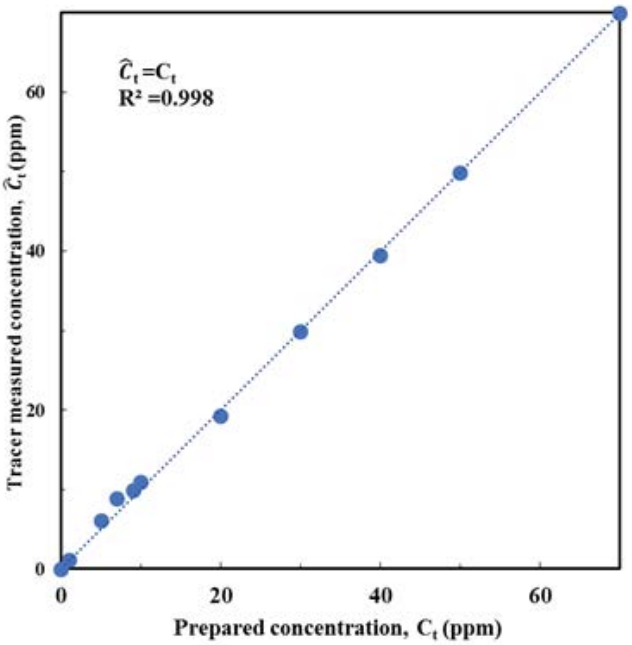

Fig. 2. Calibration curve of the tracer solution concentration.

2.3. Experimental procedures

For both RO and NF modules, the first step is to determine the flow and the recovery rates at different applied trans-membrane pressures. These experiments were conducted with pure water. At each applied pressure, the experiment was repeated at least 3 times, giving a relative standard deviation lower than 5%. Once a steady state is

reached, identified by the constant flow rate and conductivity of both permeate and concentrate streams, 5 mL of the tracer was injected on a pulse step at the entrance of the (RO/NF) membrane module. The tracer concentration was 23.8 ± 0.98 mg/L.

After the tracer injection, different samples were collected at various time intervals. Tracer contents were determined using the Pen Fluorometer. This allows the obtainment of the response signal at the outlet of the membrane module. Using the relevant equations presented in the next section, the RTD distribution and its parameters were determined.

2.4. RTD equations

The RTD function or the exit age distribution, known as $E(t)$, represents the probability of the tracer that entered the process at $t = 0$ to exit it at the time t. It is given by the following expression [23,28]:

$$E(t) = \frac{C(t)}{\int_0^\infty C(t)dt} \tag{3}$$

where $C(t)$ is the tracer concentration in the retentate side at the module outlet. After a sufficient time, all the tracer material leaves the membrane module and the conservation equation is translated by the following expression:

$$\int_0^\infty E(t)dt = 1 \tag{4}$$

The area under the RTD function between time 0 and t is the fraction of the tracer that has left the system up to that time. It is defined as the cumulative distribution function $F(t)$, being therefore expressed as:

$$F(t) = \int_0^t E(t)dt \tag{5}$$

The mean residence time (MRT) known as t is a significant parameter in RTD studies. It is the first central moment of the RTD function, defined as the average time a tracer particle spends in the system. It is equal to:

$$\tau = \int_0^\infty tE(t)dt \tag{6}$$

Another important parameter is the second central moment of the RTD function termed variance s^2, which indicates the quality of the spread inside the system. A non-zero variance suggests the existence of some dispersion along the membrane, which can be caused by flow turbulence, a non-uniform velocity profile, or diffusion. Thus, the higher the value, the higher the intermixing between zones of the studied system [29]. It is depicted as:

$$\sigma^2 = \int_0^\infty (t-\tau)^2 E(t)dt \tag{7}$$

The mixing intensity can be described using the dispersion coefficient D, equivalent to the diffusion coefficient characterizing molecular mixing. The dimensionless dispersion number, which is the inverse of the Péclet number (Pe = uL/D), is given by [14]:

$$\frac{D}{uL} = \frac{1+\sqrt{1+8\frac{\sigma^2}{\tau^2}}}{8} \tag{8}$$

where u is the flow velocity and L is the module flow length.

This number indicates the mixing effects in the spiral wound module flow passages. It represents the ratio of the convective to dispersive effects. In other words, dispersion is predominant when Pe is low. When Pe is high, the dispersion is insignificant. Thus, for an ideal flow system closing to plug flow, D/uL approaches 0. For a highly mixed flow system, D/uL is infinite. The experimental data were fitted with a normal distribution function, which can be described using the mean residence time (τ) and the second central moment (s^2) as presented in the following equation:

$$f(t) = \frac{1}{\sigma^*\sqrt{2\pi}}\exp\left(-\frac{1}{2}\left(\frac{t-\tau^*}{\sigma^*}\right)^2\right) \tag{9}$$

Fitting experimental points according to Eq. (9) will allow determining τ^* and $(\sigma^*)^2$, and evaluate the adequateness of the normal distribution function by providing a coefficient of determination R^2. This coefficient assesses the ability of the model to predict the outcome, it is defined by [30]:

$$R^2 = 1 - \frac{\sum\left(f(t)-E(t)\right)^2}{\sum\left(\tau-E(t)\right)^2} \tag{10}$$

In addition to the coefficient of determination R^2, the relative difference between the experimental and the normal distribution model was used for comparison, according to the following equations:

$$\omega_\tau = \frac{\tau^*-\tau}{\tau} \tag{11}$$

$$\omega_{\sigma^2} = \frac{(\sigma^*)^2-\sigma^2}{\sigma^2} \tag{12}$$

where $\omega\tau$ and $\omega\sigma^2$ are the relative differences for the mean residence time and the variance, respectively.

For ideal CSTR or plug-flow systems, the mean residence time is equal to the nominal residence time (t_m), which is a function of the volumetric flow Q rate and the system volume V:

$$t_m = \frac{V}{Q} \tag{13}$$

As the tracer cannot permeate through the membrane, the considered volume is the volume on the concentrate side. In a membrane desalination process, as water permeates through the membrane, the volumetric flow rate on the concentrate side decreases. The mean volumetric flow rate in the feed flow direction varies with conversion rate R according to:

$$Q = \frac{1}{R}\int Q_c dR \tag{14}$$

For a single membrane module operating at low pressure, the volumetric flow rate can be expressed as:

$$Q = \frac{1}{2}\left(Q_f + Q_c\right) = \left(1 - \frac{R}{2}\right)Q_f \tag{15}$$

The difference between the mean residence time and the nominal residence time reflects the presence of dead zones in membrane modules. The dead volume fraction inside membrane modules is given by:

$$F_v = 1 - \frac{\tau}{t_m} \tag{16}$$

The ratio of the square root of the variance, known as standard deviation, to the mean is an important parameter called the coefficient of variation.

$$C_v = \frac{\sigma}{\tau} \tag{17}$$

This coefficient gives a measure of the relative size of the dispersion zone compared to the module length. It indicates the presence of total tracer dispersion when it is equal to 1. However low values indicate a narrower RTD, and therefore a better radial mixing quality with a flow approaching a plug flow regime [31,32].

The third moment of the RTD function termed skewness λ_3, can outline the symmetry of the distribution depending on the degree of positivity or negativity. A positive value means that part of the tracer is skipping the mixing zone, thus traveling faster than the bulk flow. This positive value may be due to the presence of important dead zones. A negative value points that part of the tracer is trapped in the system. As the majority of the tracer drifts slower than the average, the distribution will show a tail on the left-hand side [24,33]. This can be caused by the presence of large internal recirculation zones.

$$\lambda_3 = \frac{1}{\sigma^3}\int_0^\infty \left(t - \tau\right)^3 E\left(t\right)dt \tag{18}$$

3. Results

RTD measurements using a laboratory pilot unit were performed for RO and NF modules as described in section 2. The variations of RTD within trans-membrane pressure intervals were determined. The experimental results were exploited using the theoretical developments described in section 2.4.

3.1. Recovery rates

Fig. 3 shows the recovery rate of NF and RO modules as functions of the applied pressure. It is clear that at the same applied pressure, the recovery rate of the NF module is higher compared to the RO module. This is the result of the difference in membrane permeability, as the NF membrane has greater pore sizes.

3.2. RTD determination

The RTD plays an important role in flow hydrodynamics characterization as it relates to the mixing conditions. RTD curves vary from very narrow, symmetric distributions (plug flow) when there is substantial radial mixing, to the other extreme RTDs approximating those of continuous stirred tanks, when radial mixing is poor. A narrow RTD is normally preferred in membrane modules, and therefore a lower variance is favored. Following the procedure described in section 2.2, RTD test results at three different pressures using the RO and NF modules are displayed in Fig. 4. For each trans-membrane pressure, a representative curve is shown. In all investigated cases, the relative standard deviation for each replications series remained below 4%.

A slightly asymmetrical distribution with a relatively long tail on the right was observed at different applied pressures. The long-tail phenomenon reveals an anomalous transport behavior, well documented in tracer transport in porous media and commonly referred to as the non-Fickian

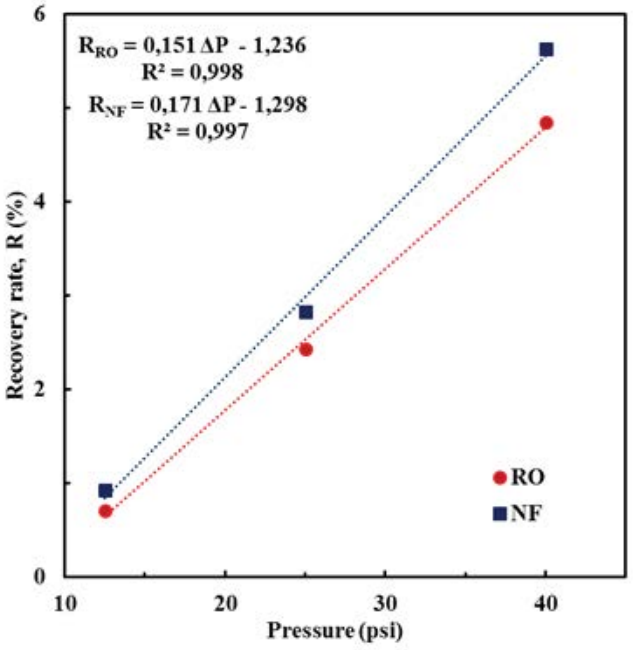

Fig. 3. Recovery rate as functions of the applied pressure for domestic size NF and RO modules.

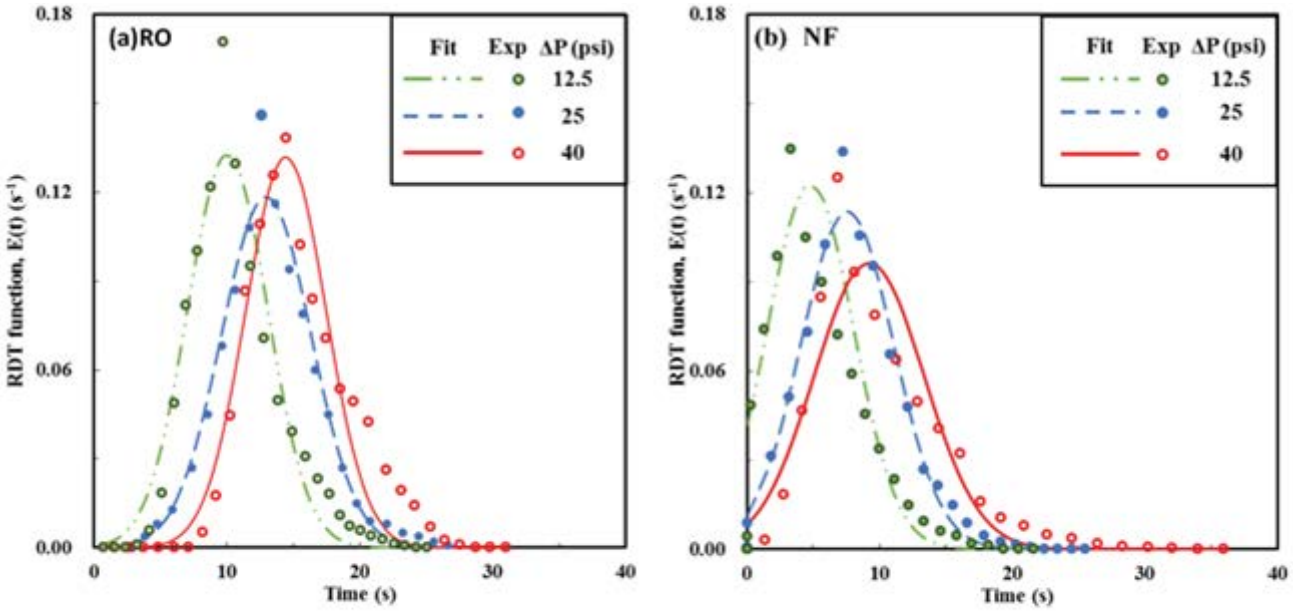

Fig. 4. Residence time distribution functions for domestic size (a) RO and (b) NF modules at three different applied pressures (12.5, 25 and 40 psi).

behavior [34,35]. For a membrane module, the tail could have several origins. Two of which are more likely:

- The tracer might have an affinity with the active layer and/or the spacer and/or any deposited fouling material on the active layer of the membrane, which slightly hinders its transport.
- Dead zones, located at the contact areas between the spacer and membrane, could momentarily trap some tracer molecules.

Both phenomena could contribute to this non-Fickian behavior. Most likely, dead volumes are responsible for the tail appearance. For the RO module, the peak of the RTD function occurs later with the increase of the applied pressure. $E(t)$ maximum at 12.5 psi happens at 8 s, while at 40 psi, the RTD function reaches its maximum at approximately 15 s. The NF module results resemble the ones obtained with the RO module but showing slightly more positively skewed curves which shift to the right with the increase of the applied pressure. Moreover, the RTD function peak occurs earlier compared to the RO module. In the NF module, $E(t)$ maximum at 12.5 psi happens at 3.3 s, while at 40 psi, it happens at 8.22 s.

According to the cumulative distribution function shown in Fig. 5 in the case of RO, half of the injected tracer exits the module at 9.63, 12.25, and 14.38 s, corresponding to the applied pressure of 12.5, 25, and 40 psi, respectively. On the other hand, 90% of the injected tracer comes out of the NF module at 10, 11.72, and 14.41 s with an applied pressure of 12.5, 25 and, 40 psi, respectively. At those instants, only around 50% of the injected tracer leaves the RO module for the same applied pressures. Increasing the applied pressure delays the tracer particle exit time.

3.3. RTD parameters

The trans-membrane pressure effects on the mean residence time (t), obtained using equation 6 for NF and RO modules, are shown in Fig. 6. The figure manifests a near-perfect linear increasing behavior of the mean residence time as the pressure rise, with very close slopes for both NF and RO modules. It also shows that the tracer spends a much longer time inside the RO module compared to the NF module.

The mean residence time is longer compared to the observed peak time. For RO, there is a lateness of about 2.95 and 0.7 s at 12.5 and 40 psi, respectively. For NF, the delay varies from 2 to 1.28 s from 12.5 to 40 psi, respectively. This belatedness suggests the presence of stagnant volumes for both NF and RO modules. There is a difference of about 5.9 ± 0.3 s between RO and NF mean residence times. This difference is due to the higher permeate flow in the NF module compared to the RO module mainly because of the characteristics of the membranes, as discussed previously.

Fig. 7 shows the variation of the second central moment (σ^2) values, which have been determined following Eq. (7). Variance values increase with the applied pressure. This tendency reflects a higher axial dispersion in the flow direction within the membrane module with the increase of the applied pressure. However, the increase in the variance is matched with an increase in the mean residence time, giving an overall decrease in the variation coefficient C_v as shown in Fig. 8. This means that when increasing the applied pressure, the circulation of the concentrate inside the membrane module approaches the plug flow configuration. The variation is prominent in the case of the NF membrane, because of its higher permeability compared to the RO membrane. This is further demonstrated by the decrease in the dispersion number as the pressure increases. Fig. 9 depicts the

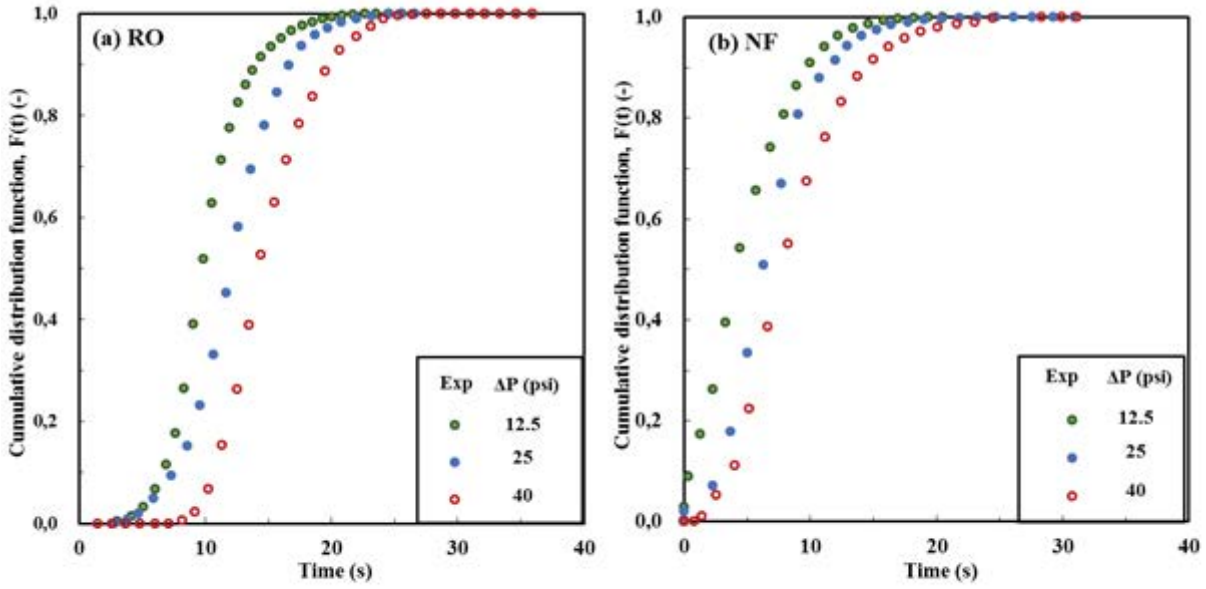

Fig. 5. Cumulative distribution function for domestic size (a) RO and (b) NF tests at three different applied pressures (12.5, 25 and 40 psi).

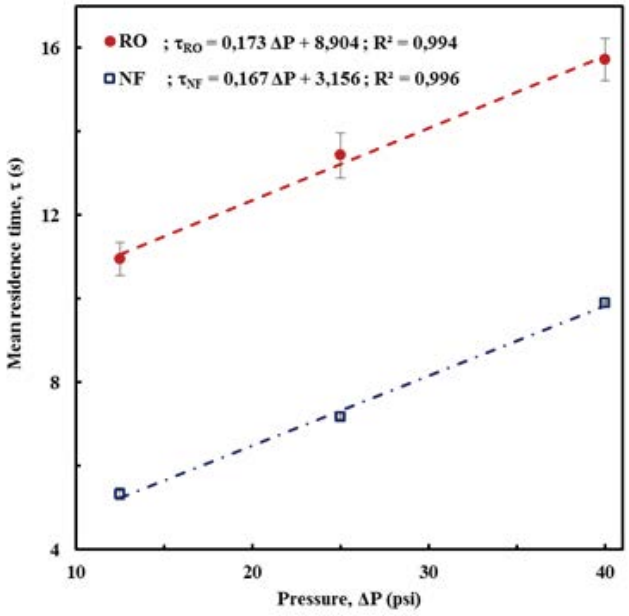

Fig. 6. Experimental mean residence time as function of the applied pressure for domestic size NF and RO.

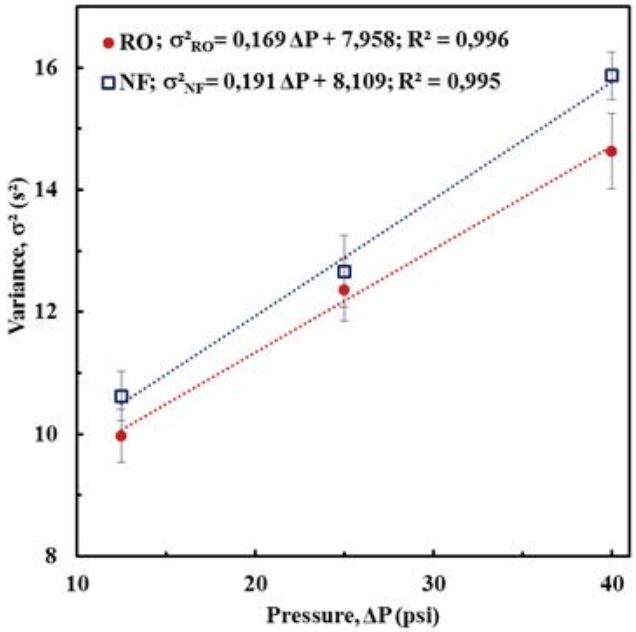

Fig. 7. Experimental second central moment (τ²) as function of the applied pressure for domestic size NF and RO.

dispersion number at three different pressures for the RO and NF units. It shows that raising the applied pressure leads to a lower dispersal effect. This figure also displays the difference between NF and RO membranes. The dispersion is much higher and the influence of the applied pressure is more pronounced. The dispersive number was reduced by approximately 9% and 40% when the pressure changed from 12.5 to 25 psi for RO and NF membranes, respectively.

As described in section 2.4, the experimental and normal distribution model parameters for RO and NF tests were determined and compared. Table 2 shows that for all experiments, the normal distribution adequately fits the experimental data. The RTD parameters vary significantly with applied trans-membrane pressure. It is noticeable that the mean residence time obtained from the Normal distribution model is shorter than the experimental value.

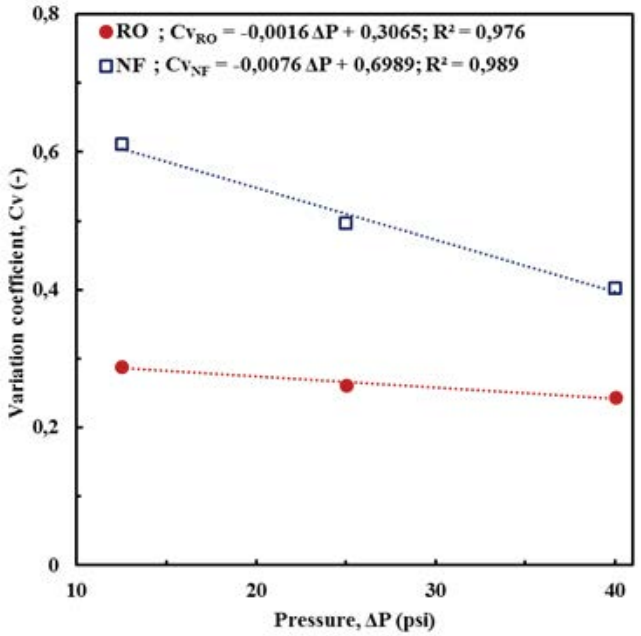

Fig. 8. Coefficient of variation as function of the applied pressure for domestic size NF and RO.

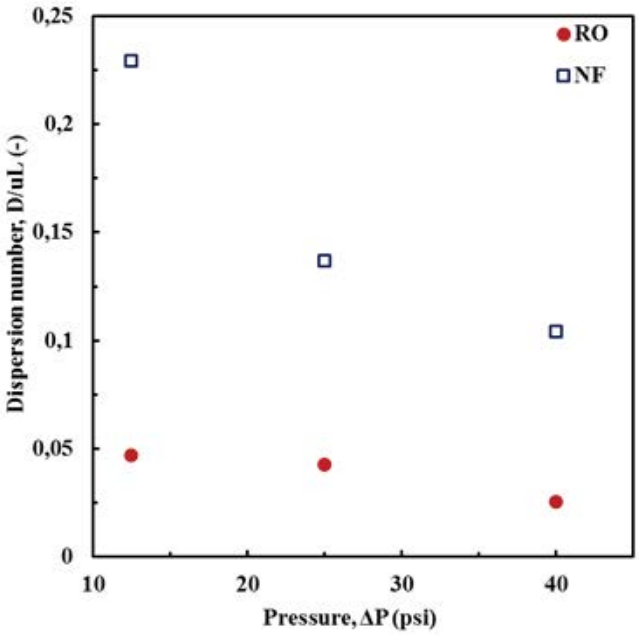

Fig. 9. The dispersion number as function of the applied pressure for NF and RO membranes.

Similarly, the experimental variance values are higher than the model-based predictions with differences exceeding 10% on average. The discrepancies are mainly due to the asymmetric distribution of the experimental data compared to the normal symmetric distribution. This asymmetry is presented in Fig. 4 by the tail skewed to the right. The different skewness values are displayed in Table 2. It is clear that the skewness degree decreases with the increase of the applied pressure. This implies that increasing the applied pressure improves the flow in the membrane module, with an RTD function approaching a normal distribution for higher applied pressures.

Likewise, normal distribution functions were used to fit the experimental data of NF tests. However, the obtained results were not as good as for RO experimental results as shown in Table 2. This can be explained by the relatively much higher positive skewness values in the NF unit compared to the RO unit. Similar to RO, skewness values decrease with the increase of the applied pressure. This decrease may also be the result of the improvement in the concentrate flow pattern with the pressure boost.

The variance values are higher in the NF module indicating a much larger dispersion in NF compared to RO. Thus, for the investigated pressure, the RO module has a lower axial dispersion giving variation coefficients smaller than the NF module. This difference is the result of the lower concentrate mean flow rate in an NF module because of the higher permeability of the membrane.

3.4. Nominal residence time

Fig. 10 shows the nominal residence time (t_m) and the experimental mean resident time (t) as functions of the applied pressure, for both NF and RO modules. The nominal residence time is obtained using Eqs. (13)–(15), accounting for approximate values of concentrate side volumes in the module. For both RO and NF modules, it is clear that there are no major differences between the mean residence time and the nominal residence time. The biggest difference is for lower pressures in the case of the NF module. The significant difference indicates the presence of large dead volumes within the membrane volume. Dead zones result from poor mixing in flow domains within process vessels [36–38]. In membrane modules, dead zones form at confined flow regions mostly located at intersections of spacer filaments and contact surfaces between the feed spacer and membranes [39,40]. Typically, feed spacers create flow channels, promote fluid mixing and improve mass transfer. However, if their design is not met with an optimized flow configuration, unfavorable flow hydrodynamics could arise possibly inducing dead zones. These dead volumes are hotspot locations for high CP phenomenon triggering scaling and fouling that extend beyond stagnation zones. As a result, fluid flow trajectory at the feed side is hindered, and preferential channels are created [41,42]. In order to reduce the emergence of dead zones, diverse spacer designs have been examined [41–43]. Dual-layer feed spacer with filament thinning zones located around the spacer junctions proved to be better than the single-layered one with non-uniform filaments [44]. In addition, perforated spacers demonstrated good results with respect to limiting stagnant zones in RO modules [45]. Fig. 11 shows the variation of the dead volume fraction (equation 15) as a function of the applied pressure. It is clear that the dead volume fraction decreases with the applied pressure, which indicates that increasing the operating pressure leads to better flow hydrodynamics inside the membrane modules. In addition, the dead volume fraction inside the NF membrane is superior to that of the RO membrane.

Table 2
Normal distribution model and experimental parameters in RO and NF experiments

	Pressure (psi)		12.5	25	40
RO	Experimental results	τ (s)	10.95 ± 0.4	13.43 ± 0.56	15.72 ± 0.50
		σ^2 (s^2)	9.97 ± 0.43	12.36 ± 0.51	14.63 ± 0.61
		λ_3 (–)	0.892 ± 0.002	0.651 ± 0.032	0.511 ± 0.035
	Model parameters	τ (s)	10.42 ± 0.05	12.83 ± 0.07	15.04 ± 0.11
		σ^2 (s^2)	7.92 ± 0.08	9.17 ± 0.11	12.17 ± 0.13
		R^2 (–)	0.994 ± 0.003	0.996 ± 0.002	0.994 ± 0.003
	Relative difference	ωτ (%)	–4.85 ± 0.38	–4.44 ± 0.39	–4.340.31
		ωσ (%)	–20.35 ± 1.98	–25.81 ± 2.44	–15.25 ± 1.43
NF	Experimental results	τ (s)	5.33 ± 0.15	7.16 ± 0.03	9.90 ± 0.01
		σ^2 (s^2)	10.62 ± 0.40	12.67 ± 0.58	15.87 ± 0.39
		λ_3 (–)	1.021 ± 0.049	0.864 ± 0.036	0.722 ± 0.048
	Model parameters	τ (s)	5.10 ± 0.25	7.21 ± 0.11	9.08 ± 0.18
		σ^2 (s^2)	8.52 ± 0.28	12.32 ± 0.19	15.67 ± 0.12
		R^2 (–)	0.966 ± 0.01	0.0979 ± 0.007	0.987 ± 0.012
	Relative difference	ωτ (%)	–4.30 ± 0.45	0.68 ± 0.02	–8.31 ± 0.18
		ωσ (%)	–19.81 ± 2.14	–2.73 ± 0.29	–1.23 ± 0.07

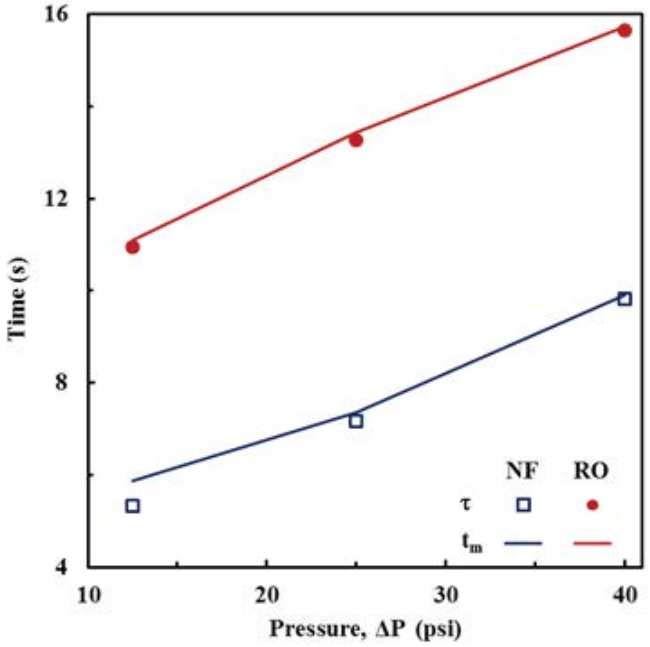

Fig. 10. Nominal residence time (t_m) and mean residence time (τ) for domestic size NF and RO units as functions of the applied pressure.

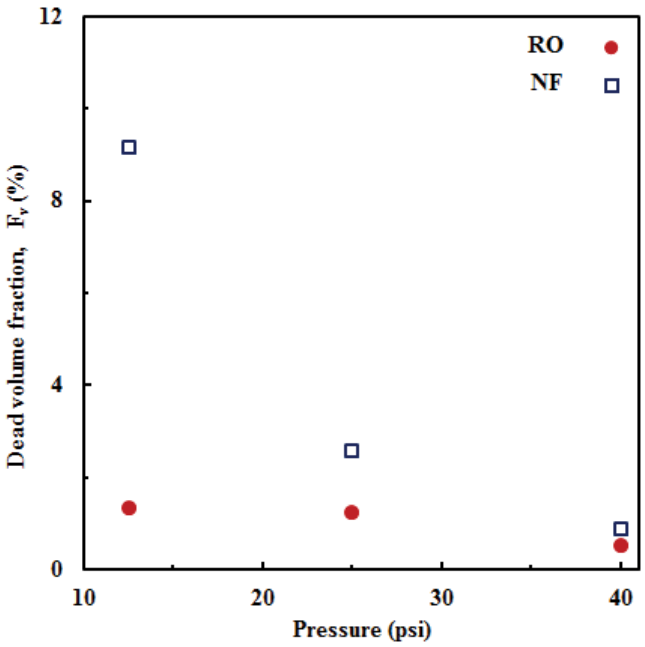

Fig. 11. Dead volume fraction for NF and RO modules as function of the applied pressure.

4. Conclusion

The purpose of this work was to unfold the RTD variation with the applied trans-membrane pressure for RO and NF modules in the case of a laboratory-scale pilot unit. The idea was to characterize the flow hydrodynamics within a domestic-sized RO/NF membrane module. For the investigation, pure water and commercial scale-inhibitor PermaTreat® PC-191T were used as a feed solution and a tracer, respectively. It was found that increasing the applied pressure leads to prolonged mean residence time and narrower axial dispersion inside the RO/NF modules. Thus, the hydrodynamics inside the membrane module approaches the favorable plug flow system for higher trans-membrane pressures. Due to their membrane characteristics, NF modules have lower mean residence times and larger axial dispersion. The observed RTDs for both NF and RO modules were consistent with the normal distribution model. With a more pronounced positive skewness, the normal distribution fitting of the experimental data for the NF module was

not as good as for the RO module, indicating the presence of significant dead volumes. From a flow hydrodynamics perspective, the applied conditions do not show an optimal configuration that might be sought in industrial membrane modules and pressure vessels. The approach implemented in this work for flow characterization in RO and NF modules could be extended to larger membrane modules and pressure vessels. It can be used to assess fouling in pressure-driven membrane processes. Most importantly, it can be used in conjunction with spacer and pressure vessel configurations and designs for better-optimized membrane separation processes.

Abbreviations

CSTR	—	Continuous stirred tank reactor
MRT	—	Mean residence time
NF	—	Nanofiltration
RO	—	Reverse osmosis
RTD	—	Residence time distribution
TDS	—	Total dissolved salts
UF	—	Ultrafiltration

Symbols

C	—	Concentration, g/m^3
C_v	—	Variation coefficient, –
D	—	Dispersion coefficient, m^2/s)
D/uL	—	Dispersion number, –
E	—	Residence time distribution function, s^{-1}
f	—	Normal distribution function, s^{-1}
F	—	Cumulative distribution function, –
F_v	—	Dead volume fraction, –
L	—	Module length, m
ΔP	—	Applied pressure, psi
Q	—	Volumetric flow rate, m^3/s
R	—	Recovery rate, %
R^2	—	Coefficient of determination, –
t	—	Time, s
t_m	—	Nominal residence time, s
u	—	Flow velocity, m/s
V	—	Module volume, m^3

Greek

l_3	—	Skewness degree, –
s^2	—	Variance, s^2
τ	—	Mean residence time, s
ω	—	Relative difference, %

Subscripts

c	—	Draw
f	—	Feed
p	—	Permeate

References

[1] SDG 6 Synthesis Report 2018 on Water and Sanitation, n.d. Available at: https://www.unwater.org/publications/sdg-6-synthesis-report-2018-on-water-and-sanitation/ (Accessed September 2, 2021).

[2] M. Sarai Atab, A.J. Smallbone, A.P. Roskilly, An operational and economic study of a reverse osmosis desalination system for potable water and land irrigation, Desalination, 397 (2016) 174–184.

[3] K. Minyaoui, H. Hchaichi, P. Maxime, A. Hannachi, Integrated approach for brackish water desalination and distribution: Which desalination technology to choose?, Desal. Water Treat., 73 (2017) 121–126.

[4] A. Alkaisi, R. Mossad, A. Sharifian-Barforoush, A review of the water desalination systems integrated with renewable energy, Energy Procedia, 110 (2017) 268–274.

[5] S.F. Anis, R. Hashaikeh, N. Hilal, Reverse osmosis pretreatment technologies and future trends: a comprehensive review, Desalination, 452 (2019) 159–195.

[6] J. Bohdziewicz, M. Bodzek, E. Wąsik, The application of reverse osmosis and nanofiltration to the removal of nitrates from groundwater, Desalination, 121 (1999) 139–147.

[7] A. Lhassani, M. Rumeau, D. Benjelloun, M. Pontie, Selective demineralization of water by nanofiltration application to the defluorination of brackish water, Water Res., 35 (2001) 3260–3264.

[8] A. M'nif, S. Bouguecha, B. Hamrouni, M. Dhahbi, Coupling of membrane processes for brackish water desalination, Desalination, 203 (2007) 331–336.

[9] N. Ghaffour, T.M. Missimer, G.L. Amy, Technical review and evaluation of the economics of water desalination: current and future challenges for better water supply sustainability, Desalination, 309 (2013) 197–207.

[10] H. Hchaichi, S. Siwar, H. Elfil, A. Hannachi, Scaling predictions in seawater reverse osmosis desalination, Membr. Water Treat., 5 (2014) 221–233.

[11] H. Elfil, A. Hamed, A. Hannachi, Technical evaluation of a small-scale reverse osmosis desalination unit for domestic water, Desalination, 203 (2007) 319–326.

[12] A. Antony, J.H. Low, S. Gray, A.E. Childress, P. Le-Clech, G. Leslie, Scale formation and control in high pressure membrane water treatment systems: a review, J. Membr. Sci., 383 (2011) 1–16.

[13] S. Jiang, Y. Li, B.P. Ladewig, A review of reverse osmosis membrane fouling and control strategies, Sci. Total Environ., 595 (2017) 567–583.

[14] O. Levenspiel, Chemical Reaction Engineering, John Wiley & Sons, Hoboken, New Jersey, USA, 1998.

[15] S. Rjeb, A. Hannachi, R. Abdelhamid, Hydrodynamic investigation in an annular reactor with mixing time and residence time distribution: flow rates estimation with the gauss-newton gradient technique, Chem. Prod. Process Model., 6 (2011), doi: 10.2202/1934-2659.1539.

[16] E. Roth, M. Kessler, B. Fabre, A. Accary, Sodium chloride stimulus-response experiments in spiral wound reverse osmosis membranes: a new method to detect fouling, Desalination, 121 (1999) 183–193.

[17] P. Dydo, M. Turek, J. Ciba, Laboratory RO and NF processes fouling investigation by residence time distribution curves examination, Desalination, 164 (2004) 33–40.

[18] D. Hasson, A. Drak, C. Komlos, Q. Yang, R. Semiat, Detection of fouling on RO modules by residence time distribution analyses, Desalination, 204 (2007) 132–144.

[19] Q. Yang, A. Drak, D. Hasson, R. Semiat, RO module RTD analyses based on directly processing conductivity signals, J. Membr. Sci., 306 (2007) 355–364.

[20] A. Miskiewicz, G. Zakrzewska-Trznadel, A. Dobrowolski, A. Jaworska-Sobczak, Using tracer methods and experimental design approach for examination of hydrodynamic conditions in membrane separation modules, Appl. Radiat. Isot., 70 (2012) 837–847.

[21] T.Y. Qiu, P.A. Davies, Longitudinal dispersion in spiral wound RO modules and its effect on the performance of batch mode RO operations, Desalination, 288 (2012) 1–7.

[22] M. Li, Residence time distribution in RO channel, Desalination, 506 (2021) 115000, doi: 10.1016/j.desal.2021.115000.

[23] M. Sheoran, A. Chandra, H. Bhunia, P.K. Bajpai, H.J. Pant, Residence time distribution studies using radiotracers in

chemical industry—a review, Chem. Eng. Commun., 205 (2018) 739–758.
[24] A. Bérard, B. Blais, G.S. Patience, Experimental methods in chemical engineering: residence time distribution—RTD, Can. J. Chem. Eng., 98 (2020) 848–867.
[25] A.E. Rodrigues, Residence time distribution (RTD) revisited, Chem. Eng. Sci., 230 (2021) 116188, doi: 10.1016/j.ces.2020.116188.
[26] N. Meftah, A. Ezzeddine, A. Bedoui, A. Hannachi, Hybrid neutralization and membrane process for fluoride removal from an industrial effluent, Membr. Water Treat., 11 (2020) 303–312.
[27] N. Meftah, A. Ezzeddine, A. Bedoui, A. Hannachi, Nanofiltration polishing membrane process for fluoride removal, Desal. Water Treat., 198 (2020) 90–97.
[28] H.S. Fogler, Elements of chemical reaction engineering, Chem. Eng. Sci., 42 (n.d.) 2493.
[29] M. Dülle, H. Özcoban, C.S. Leopold, The effect of different feed frame components on the powder behavior and the residence time distribution with regard to the continuous manufacturing of tablets, Int. J. Pharm., 555 (2019) 220–227.
[30] D. Chicco, M.J. Warrens, G. Jurman, The coefficient of determination R-squared is more informative than SMAPE, MAE, MAPE, MSE and RMSE in regression analysis evaluation, PeerJ Comput. Sci., 7 (2021) e623, doi: 10.7717/peerj-cs.623.
[31] D.A. Sievers, J.J. Stickel, Modeling residence-time distribution in horizontal screw hydrolysis reactors, Chem. Eng. Sci., 175 (2018) 396–404.
[32] L. Hua, J. Wang, Residence time distribution of particles in circulating fluidized bed risers, Chem. Eng. Sci., 186 (2018) 168–190.
[33] M. Sebastian Escotet-Espinoza, S. Moghtadernejad, S. Oka, Y. Wang, A. Roman-Ospino, E. Schäfer, P. Cappuyns, I. Van Assche, M. Futran, M. Ierapetritou, F. Muzzio, Effect of tracer material properties on the residence time distribution (RTD) of continuous powder blending operations. Part I of II: experimental evaluation, Powder Technol., 342 (2019) 744–763.
[34] B. Berkowitz, H. Scher, S.E. Silliman, Anomalous transport in laboratory-scale, heterogeneous porous media, Water Resour. Res., 36 (2000) 149–158.
[35] B. Bijeljic, S. Rubin, H. Scher, B. Berkowitz, Non-Fickian transport in porous media with bimodal structural heterogeneity, J. Contam. Hydrol., 120–121 (2011) 213–221.
[36] N.K. Karadimitriou, V. Joekar-Niasar, M. Babaei, C.A. Shore, Critical role of the immobile zone in non-fickian two-phase transport: a new paradigm, Environ. Sci. Technol., 50 (2016) 4384–4392.
[37] R.E. Hayes, J.P. Mmbaga, Introduction to Chemical Reactor Analysis, CRC Press, Boca Raton, Florida, USA, 2012.
[38] T. Matsuo, K. Hanaki, S. Takizawa, H. Satoh, Advances in Water and Wastewater Treatment Technology: Molecular Technology, Nutrient Removal, Sludge Reduction, and Environmental Health, Elsevier, Amsterdam, Netherlands, 2001.
[39] T. Ishigami, H. Matsuyama, Numerical modeling of concentration polarization in spacer-filled channel with permeation across reverse osmosis membrane, Ind. Eng. Chem. Res., 54 (2015) 1665–1674.
[40] S.J. Altman, L.K. McGrath, H.D.T. Jones, A. Sanchez, R. Noek, P. Clem, A. Cook, C.K. Ho, Systematic analysis of micromixers to minimize biofouling on reverse osmosis membranes, Water Res., 44 (2010) 3545–3554.
[41] W. Lin, Y. Zhang, D. Li, X. Wang, X. Huang, Roles and performance enhancement of feed spacer in spiral wound membrane modules for water treatment: a 20-year review on research evolvement, Water Res., 198 (2021) 117146, doi: 10.1016/j.watres.2021.117146.
[42] R. Rahmawati, M.R. Bilad, N.I.M. Nawi, Y. Wibisono, H. Suhaimi, N. Shamsuddin, N. Arahman, Engineered spacers for fouling mitigation in pressure driven membrane processes: progress and projection, J. Environ. Chem. Eng., 9 (2021) 106285, doi: 10.1016/j.jece.2021.106285.
[43] M.R. Cruz-Díaz, A. Laureano, F.A. Rodríguez, L.F. Arenas, J.J.H. Pijpers, E.P. Rivero, Modelling of flow distribution within spacer-filled channels fed by dividing manifolds as found in stacks for membrane-based technologies, Chem. Eng. J., 423 (2021) 130232, doi: 10.1016/j.cej.2021.130232.
[44] W. Lin, R. Shao, X. Wang, X. Huang, Impacts of non-uniform filament feed spacers characteristics on the hydraulic and anti-fouling performances in the spacer-filled membrane channels: Experiment and numerical simulation, Water Res., 185 (2020) 116251, doi: 10.1016/j.watres.2020.116251.
[45] S. Kerdi, A. Qamar, J.S. Vrouwenvelder, N. Ghaffour, Fouling resilient perforated feed spacers for membrane filtration, Water Res., 140 (2018) 211–219.